Chemical Physics 348 (2008) 143–151

Contents lists available at ScienceDirect

Chemical Physics

journal homepage: www.elsevier.com/locate/chemphys

Comparison of nonlinear absorption in three similar dyes: Polymethine, squaraine and tetraone

Scott Webster [a,*], Jie Fu [a], Lazaro A. Padilha [a], Olga V. Przhonska [a,b], David J. Hagan [a,c], Eric W. Van Stryland [a,c], Mikhail V. Bondar [b], Yuriy L. Slominsky [d], Alexei D. Kachkovski [d]

[a] CREOL, & FPCE, The College of Optics and Photonics, University of Central Florida, FL 32816-2700, United States
[b] Institute of Physics, National Academy of Sciences, Prospect Nauki 46, Kiev 03028, Ukraine
[c] Department of Physics, University of Central Florida, FL 32816-2700, United States
[d] Institute of Organic Chemistry, National Academy of Sciences, Murmanskaya 5, Kiev 03094, Ukraine

ARTICLE INFO

Article history:
Received 20 June 2007
Accepted 25 February 2008
Available online 8 March 2008

Keywords:
Polymethine
Squaraine
Tetraone
Two-photon absorption
Excited-state absorption
Cyanine

ABSTRACT

We performed a detailed experimental investigation and quantum-chemical analysis of two-photon absorption (2PA) spectra of symmetrical cationic polymethine and neutral squaraine and tetraone dyes having nearly identical terminal groups and similar conjugation length. Squaraine and tetraone structures differ from polymethines in that their conjugated backbone includes an electron accepting bridge. Frequency degenerate 2PA spectra of these molecules are measured by two-photon fluorescence spectroscopy and the *Z*-scan technique. Comparing 2PA spectra of polymethine with squaraine and tetraone structures, we find that we can access considerably larger 2PA cross-sections ($\geqslant 8000 \times 10^{-50}$ cm^4 s/photon) in the squaraine and tetraone molecules due to an increase in the density of final states introduced by the electron accepting bridge in the conjugated chain. We discuss the difference in electronic structure for these molecules and introduce a link between 2PA and excited-state absorption spectra. The results of these experiments combined with agreement of quantum-chemical calculations moves us closer to a predictive capability for the relation between molecular structure and nonlinear optical properties.

1. Introduction

Nonlinear optical applications based on organics, including optical recording media, nonlinear microscopy and optical switching, require systematic development and characterization before practical devices can be constructed. In the past several years, polymethine (PD) and squaraine (SD) dyes have been studied extensively by our group in an effort to understand structure–property relationships for the systematic development of tailored organic nonlinear optical absorbing dyes [1–5]. Recent investigations show that PDs and SDs are attractive candidates for two-photon absorption (2PA) studies due to their very large ground-state transition dipole moments, near-parallel orientation of their ground and excited-state transition dipole moments, and the sharply rising low-energy side of their linear absorption spectra that allow significant intermediate state resonance enhancement (ISRE) of the 2PA [5,6]. In addition, our systematic studies of excited-state absorption (ESA) in these types of molecules [3] have added to our insight of the level structure allowing us to make links between 2PA and ESA as indicated by perturbation theory.

Polymethine molecules typically represent symmetrical or asymmetrical combinations of a π-conjugated system with electron donating (D) terminal groups: D–π–D. Non-electron-accepting bridge units can be added to the polymethine backbones in an attempt to photochemically stabilize the chain chromophores especially for PDs absorbing in the wavelength region longer than 750 nm [3]. Our investigations revealed the following trends in structure–property relations for symmetrical PDs: (1) an increase of 2PA cross-section (δ_{2PA}) upon lengthening of the polymethine chromophore; (2) an increase of δ_{2PA} with increasing donor strength of the terminal groups for the dyes of the same chain length; and (3) asymmetrical molecules show a broader and more intense first allowed 2PA band, positioned within the main absorption band [4]. Recently, we have furthered the understanding of linear and nonlinear absorption in cyanine-like structures by including a squaraine electron acceptor (A) bridge to the main conjugation backbone: D–π–A–π–D [5]. It has been shown that this quadrupolar-type arrangement of organic molecules is highly desirable to increase 2PA cross-sections [5–7]. Our comparison of 2PA spectra of several polymethines and squaraines with the same D terminal groups and length of conjugation revealed that considerably larger 2PA cross-sections can be accessed in the squaraines [5]. This effect is due to two factors: (1) narrower linear absorption

* Corresponding author. Tel.: +1 407 823 6864.
E-mail address: swebster@creol.ucf.edu (S. Webster).

0301-0104/$ - see front matter © 2008 Elsevier B.V. All rights reserved.
doi:10.1016/j.chemphys.2008.02.062

spectra allowing the use of optical frequencies closer to the linear absorption resonance (so-called intermediate state resonance enhancement, ISRE); and (2) an increase in the density of final states introduced by the squaraine acceptor group [5]. The largest δ_{2PA} values of up to $33{,}000 \times 10^{-50}$ cm^4 s/photon (33,000 GM) were recently published in Ref. [6] for extended squaraine dyes in which the terminal symmetric D groups were separated from the central squarylium A bridge by longer conjugated chromophores. In an attempt to understand the effects of the electron accepting bridge, a new D–π–A–π–D quadrupolar system containing a stronger acceptor than squaraine, a tetraone acceptor bridge, has been synthesized. Linear and nonlinear absorption properties are compared to similarly conjugated polymethine and squaraine structures with benzoindolium terminal groups.

In this work, we describe a detailed experimental investigation and quantum-chemical analysis of cationic polymethine and two neutral squaraine and tetraone dyes with analogous structures to provide a deeper insight into the nature of the 2PA and ESA processes. We discuss the difference in electronic structure for these molecules and introduce a link between 2PA and ESA spectra. In the following sections we describe: (1) the structure and one-photon (1PA) absorption properties of polymethine, squaraine and tetraone molecules; (2) the experimental methods used for 2PA and ESA measurements; (3) a detailed analysis of the 2PA spectra; and (4) their quantum-chemical modeling allowing us to understand the nature of the 2PA bands. We find that we can experimentally access larger 2PA cross-sections in squaraine and tetraone dyes than in polymethines due to an extra 2PA band caused by acceptor groups in the conjugated chains. The combination of these studies of 2PA absorption, our earlier studies of ESA, and our quantum-chemical calculations, gives us a considerably clearer picture of structure–property relations as applied to nonlinear absorption in cyanine and cyanine-like molecules.

2. Experimental and results

2.1. Materials and linear characterization

The molecular structures of the dyes studied in this paper are shown in Fig. 1(a). Their chemical names are: 2-[5-(3-ethyl-1,3-dihydro-1,1-dimethyl-2-*H*benzo[*e*]indol-2-ylidene)-1,3-pentadienyl]-3-ethyl-1,1-dimethyl-1H-benzo[*e*]indolium *p*-toluen sulfonate (labeled as PD 2630); 2-[(3-butyl-1,1-dimethyl-1,3-dihydro-2*H*-benzo[*e*]indol-2-ylidene)methyl]-4-[(3-butyl-1,1-dimethyl-1*H*-benzo[*e*]indol-2-yl) methylene]-3-oxocyclobut-1-en-1-olate (labeled as SD 2243) and 3,6-bis[2-(3-butyl-1,3-dihydro-1,1-dimethyl-2H-benzo[*e*]indol-2- ylidene)ethylidene]-1,2,4,5-cyclohexanetetrone (labeled as TD 2765). The extinction coefficients are: 2.12×10^5 M^{-1} cm^{-1} at a peak position of 682 nm for PD 2630 in ethanol; 3.45×10^5 M^{-1} cm^{-1} at a peak position of 668 nm for SD 2243 in dichloromethane and 2.309×10^5 M^{-1} cm^{-1} at a peak position of 624 nm for TD 2765 in ethanol. The linear and nonlinear measurements for SD 2243 are measured in dichloromethane, as it does not dissolve well in ethanol. These molecules possess nearly identical benzoindolium terminal groups and similar lengths of conjugation for the purpose of having a simplified, comparative analysis of the influence of increasing the acceptor bridge strength on the nonlinear optical properties.

The linear absorption spectra of the molecules, recorded with a Varian Cary 500 spectrophotometer, are shown in Fig. 1(b). As can be seen, the absorption spectra of SD 2243 and TD 2765 are blue shifted with increasing electron acceptor strength. This correlates to a decrease in effective conjugation length due to bond lengthening in the acceptor groups when compared to the unsubstituted PD 2630. PD 2630 and SD 2243 have the same polymethine chain length with an odd number of carbon atoms. The tetraone dye exhibits a more pronounced vibronic structure in the absorption band, which is typical for a polyene-like compound with an even number of carbon atoms in the conjugated chain. Both tetraone and squaraine dyes are characterized by a steeper long wavelength linear absorption edge, allowing closer tuning of the one-photon resonance. This is important for maximizing ISRE. Values for the transition dipole moments μ_{01} for the molecules are calculated from the integrated main absorption band $S_0 \rightarrow S_1$ [8]: $\mu_{01} = \{[1500(\hbar c)^2 \ln 10] \int \varepsilon_{01}(\nu) d\nu]/\pi N_A E_{01}\}^{1/2}$, where $\varepsilon_{01}(\nu)$ is the extinction coefficient, N_A is Avogadro's number, and E_{01} is the peak energy. Calculations show that all dyes have very similar μ_{01} values: 13 D for TD 2765, 13.8 D for SD 2243 and 14 D for PD 2630. This indicates that the increase in 2PA with the addition of an acceptor bridge is not due to the μ_{01} transition dipole moments.

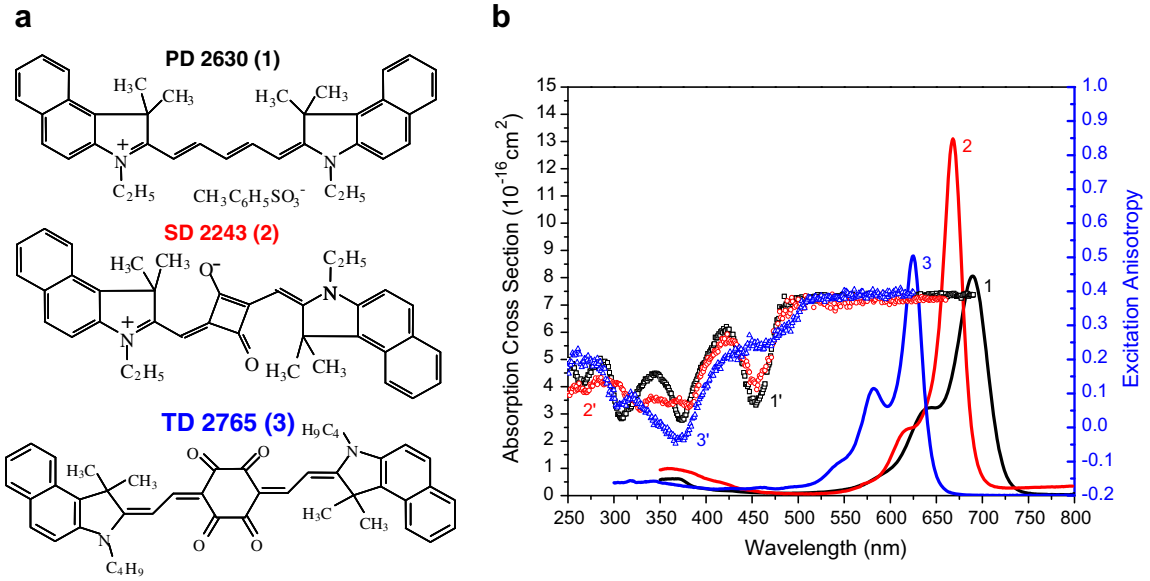

Fig. 1. (a) Molecular structures for PD 2630 (1), SD 2243 (2), and TD 2765 (3). (b) Linear absorption spectra for PD 2630 in ethanol (1), SD 2243 in dichloromethane (2), and TD 2675 in ethanol (3). Also presented are excitation anisotropy spectra in glycerol (1′, 2′, 3′ in the corresponding order).

The spectral positions of the optical transitions along with the dye energy levels and orientation of the transition dipole moments can be determined by one-photon excitation anisotropy measurements. These measurements are performed using a PTI Quantamaster Spectrofluorimeter in glycerol solutions to avoid rotational reorientation and at low concentrations ($C \approx 10^{-6}$ M) to avoid re-absorption of the fluorescence. Anisotropy values $r(\lambda)$ are calculated as $r(\lambda) = \frac{I_{\parallel}(\lambda) - I_{\perp}(\lambda)}{I_{\parallel}(\lambda) + 2I_{\perp}(\lambda)}$ by setting the emission wavelength near the fluorescence maximum with a fixed polarization. We then measure the fluorescence intensity as a function of excitation wavelength at polarization parallel, $I_{\parallel}(\lambda)$, and perpendicular, $I_{\perp}(\lambda)$, to the emission polarization. Detailed information about this technique can be found in Ref. [9]. Also, our previous studies of anisotropy in PDs and SDs are analyzed in Refs. [1,2,5]. As shown in Fig. 1(b), one-photon excitation anisotropy spectra reveal the alternation of the allowed and forbidden symmetry of one-photon transition bands; however, this information cannot be fully obtained from the linear absorption spectra. Analysis of the one-photon anisotropy spectra, especially when linked to quantum-chemical calculations, can indicate the positions of one-photon forbidden transitions, i.e. transitions between states of the same symmetry, and therefore, possible positions of 2PA bands. As can be seen from Fig. 1(b), $r(\lambda) = 0.4$ in the spectral range 500–650 nm for all dyes indicating the parallel orientation of the absorption and the emission dipole moments within the main band. In the shorter wavelength region, anisotropy spectra of PD 2630 and SD 2243 are very similar; however, they differ from the anisotropy of TD 2765 which shows no decrease in the region between 425 and 475 nm. This difference in anisotropy may be connected with the overlapping of several absorption bands, see Section 3.2.3 for details.

2.2. Nonlinear characterization

Nonlinear optical characterization (2PA and ESA spectra, as well as picosecond excited-state dynamics) of these dyes are performed using laser systems with femtosecond and picosecond pulsewidths. The femtosecond laser system consists of a Clark-MXR 2001 Ti:sapphire regeneratively amplified laser operating at 1 kHz (~1 mJ per pulse) pumping two optical parametric generator/amplifiers (Light Conversion Ltd., model TOPAS), providing 100–140 fs pulsewidths (FWHM) with independently tunable wavelengths from 0.4 to 2 μm. Temporal characteristics are measured with a GRENOUILLE (Newport, UPM-50-105) and by interferometric autocorrelation [10]. The picosecond laser system consists of a 10 Hz Nd:YAG laser (EKSPLA, model PL2143) with a pulsewidth of 21 ps (FWHM) at 1064 nm and externally frequency doubled to produce 532 nm with a pulsewidth of 15 ps (FWHM). Temporal pulsewidths are measured by second-order autocorrelations using second harmonic generation from a BBO crystal for each respective input wavelength.

Frequency degenerate 2PA spectra of the sample solutions are measured by two methods: single-wavelength open aperture *Z*-scan [11], and two-photon fluorescence (2PF) [12]. The *Z*-scan technique allows for the absolute determination of 2PA cross-sections. Focused spot sizes are calibrated at each wavelength by measuring and modeling the nonlinear refraction of a neat solution of carbon disulfide (CS_2) by the closed aperture *Z*-scan technique [13]. Detailed descriptions of the *Z*-scan technique can be found within Refs. [11,13]. This method serves as a calibration for focused spot sizes and also as an irradiance calibration to double check the independently measured energy and temporal width of the laser pulse. The open aperture *Z*-scan method was used to measure δ_{2PA} for the stronger 2PA bands and close to the one-photon absorption edge. The more sensitive method of 2PF was applied to measure the weak 2PA bands within the first linear absorption band which is only slightly allowed for symmetrical dyes. Fluorescence quantum yields are referenced against Rhodamine 6G at extremely low concentrations to avoid re-absorption of the fluorescence (quantum yield is 0.96 in ethanol [14]). 2PA cross-sections are measured and calibrated against well-known 2PA reference standards: Fluorescein in water (pH 11) and Rhodamine B in methanol [12]. For each wavelength, we check that the fluorescence signal is quadratically dependent on incident irradiance, indicating a pure two-photon absorption process. Close to the absorption tail, linear absorption affects the 2PF signal and this method cannot be used. The *Z*-scan method is required in this region since linear absorption may be more easily accounted for. However, linear absorption can produce excited-state absorption, a sequential two-photon process which gives a *Z*-scan signal similar to that of instantaneous 2PA. In the past few years, several research groups have shown very large 2PA cross-sections, in excess of 40,000 GM, but have not always shown evidence or indicated that these results have been verified to be pure 2PA. To ensure that ESA is not influencing our 2PA results, we perform femtosecond time-resolved pump–probe experiments for each molecule. ESA typically has a relaxation time much longer than the 150 fs excitation laser pulses, while pure 2PA is an instantaneous process (also useful for determining the pulsewidth by autocorrelation when the pump and probe are degenerate). Data for TD 2765 is shown in Fig. 2. In this experiment, the probe is held fixed at 670 nm and pumped at 710, 700, and 690 nm moving closer to the absorption edge. Pumping at 710 nm, Fig. 2 (curve 1), no ESA is observed as verified by the full recovery of the probe signal within the pulse temporal length. At 700 nm, Fig. 2 (curve 2), pump–probe measurements show a small fraction of ESA (signal lasting after the pulse), indicating mostly 2PA evidenced by a recovery of ~94% of the normalized transmittance. Significant ESA is observed with a pumping wavelength of 690 nm in Fig. 2 (curve 3). At 690 nm, the linear absorption cross-section is 1.6×10^{-18} cm^2, almost three orders of magnitude smaller than the peak absorption cross-section, yet there is significant ESA. If the ESA was not accounted for in these measurements, it would have appeared that we measured a 2PA cross-section in excess of 35,000 GM and probably significantly larger even closer to the absorption edge. Experimental results for 2PA spectra are shown in Fig. 3 and discussed in Section 3.1.

To measure the ESA spectra, a femtosecond pump, with a white light continuum (WLC) probe setup is used. A description of this technique can be found in Refs. [15,16]. Briefly, the output from one of the independently tunable OPGs/OPAs is set to the absorption maximum wavelength for the pump. The second OPG/OPA is

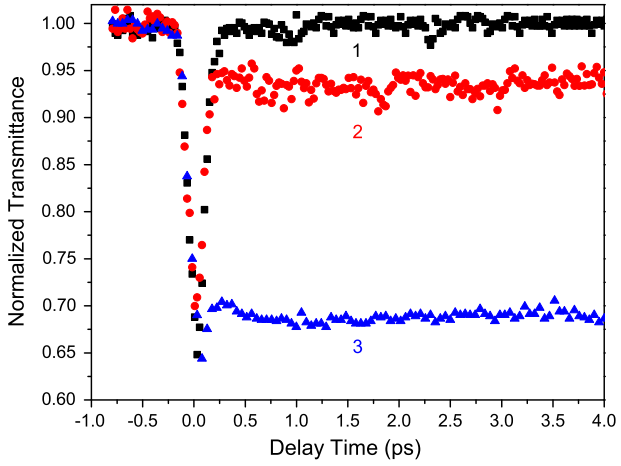

Fig. 2. Femtosecond pump–probe spectra for TD 2765. Pump wavelength is set at 670 nm and probe wavelengths are 710 nm (1), 700 nm (2), and 690 nm (3).

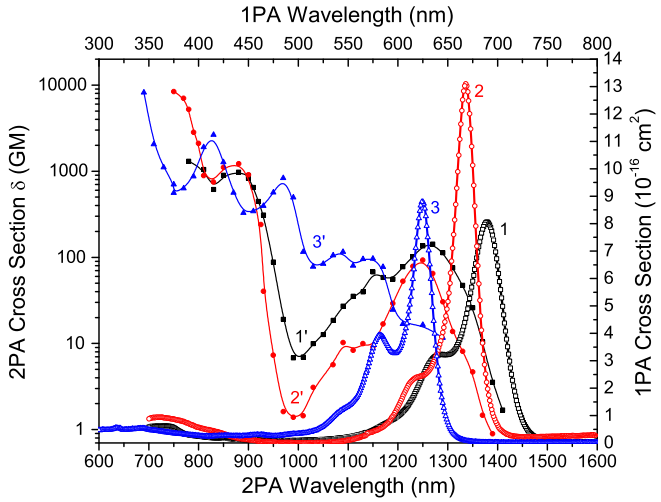

Fig. 3. One-photon absorption cross-sections (right and top axes) for PD 2630 (1), SD 2243 (2) and TD 2765 (3), and two-photon absorption cross-sections 1′, 2′, 3′, correspondingly (left and bottom axes). Uncertainties in 2PA measurements: ±20%.

sent through a calcium fluoride plate to generate a sub-picosecond white light continuum to be the probe. The probe delay time is set to 13 ps to ensure negligible contributions from vibrational relaxation while remaining shorter than the excited-state lifetime. The white light probe is then referenced and spatially overlapped with the pump in the sample and spectrally resolved upon transmission using a spectrometer (Acton Research Corp., model SpectraPro 2500i). The incident angle between pump and probe is ~5°. The ESA spectrum, $\sigma_{1i}(\lambda)$, is then calculated using Eq. (1):

$$T_L(\lambda) = \exp[-\sigma_{01}(\lambda)NL]$$
$$T_{NL}(\lambda) = \exp[-\sigma_{01}(\lambda)N_0L - \sigma_{1i}(\lambda)N_1L] \quad (1)$$

where $T_L(\lambda)$ is the linear transmittance measured by a linear spectrophotometer; $T_{NL}(\lambda)$ is the nonlinear transmittances defined by the transmittance of the probe beam in the presence of the pump; $\sigma_{01}(\lambda)$ and $\sigma_{1i}(\lambda)$ are ground and excited-state cross-sections; N is the total number of molecules per unit volume, which equals the sum of concentrations of the molecules in the ground (N_0) and the first excited state (N_1) with the approximation that we can neglect the populations of any other levels; and L is the sample length. To determine absolute values of $\sigma_{1i}(\lambda)$ in the visible region, we use $\sigma_{1i}(532)$ data obtained from the independent picosecond Z-scan measurements at 532 nm using the following equation from Ref. [16]:

$$\sigma_{1i}(\lambda) = \sigma_{01}(\lambda) - (\sigma_{01}(532) - \sigma_{1i}(532)) \times (\ln[T_{NL}/T_L]|_\lambda)/(\ln[T_{NL}/T_L]|_{532})$$

Experimentally measured ESA spectra for PD 2630, SD 2243 and TD 2765 are shown in Fig. 4 and discussed in Section 3.3.

In order to understand and model nonlinear absorption dynamics with longer picosecond pulsewidths, lifetimes of the excited-states and population dynamics must be understood. Transient picosecond polarization-resolved degenerate pump–probe studies are performed with the goal to determine fluorescence decay lifetimes, τ_F, maximum anisotropy at time $t = 0$, $r(0)$, and rotational diffusion (or reorientational) times, τ_R. These measurements are conducted at 532 nm by splitting the beam into a pump and optically delayed probe and then combining them noncollinearly in the sample at a small angle of ~5°. The pump beam diameter at focus was nearly five times larger than the low intensity probe to insure the probe experiences constant pump irradiance. Polarization dependent measurements are performed with both pump and probe parallel, perpendicular, and oriented at the "magic angle"

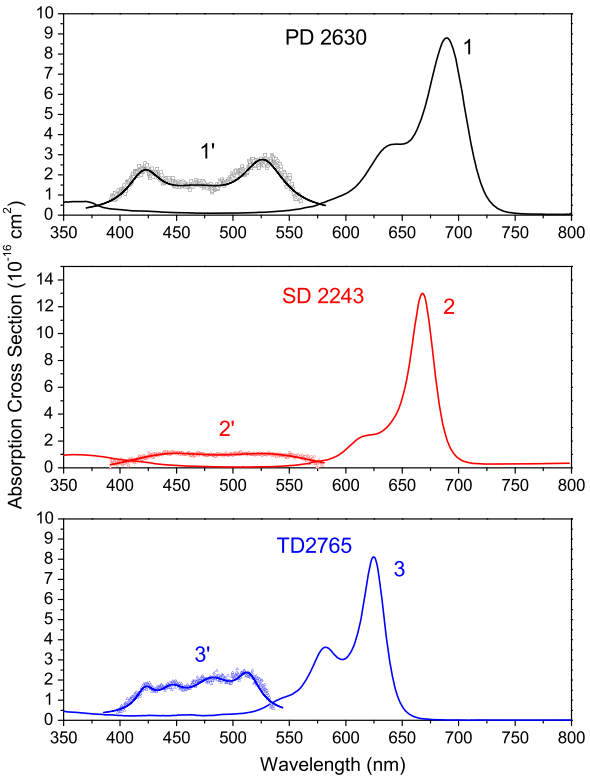

Fig. 4. Absorption cross-section for PD 2630 (1), SD 2243 (2) and TD 2765 (3), and the corresponding excited-state absorption spectra (1′), (2′), and (3′), respectively.

(54.7°). Parameters τ_F, τ_R and $r(0)$ are calculated as described in Ref. [17] by solving Eq. (2):

$$\Delta T_{\parallel}(t) = \Delta T(0)\exp(-t/\tau_F)[1 + 2r(0)\exp(-t/\tau_R)]$$
$$\Delta T_{magic}(t) = \Delta T(0)\exp(-t/\tau_F) \quad (2)$$
$$\Delta T_{\perp}(t) = \Delta T(0)\exp(-t/\tau_F)[1 - r(0)\exp(-t/\tau_R)]$$

where $\Delta T(0)$ is the change in transmittance at zero delay, $\Delta T_{\parallel}(t)$, $\Delta T_{\perp}(t)$ and $\Delta T_{magic}(t)$ are the transmittance of the probe beam at parallel, perpendicular and "magic angle" orientations, respectively. These results are presented in Fig. 5. Measurements show that $\tau_F = 2.1 \pm 0.1$ ns for both PD 2630 in ethanol and SD 2243 in dichloromethane, and the much shorter value $\tau_F = 280 \pm 50$ ps for TD 2765 in ethanol. Triplet states are not expected in this class of molecules, and it is clear from the recovery of the transmittance in Fig. 5 that triplet states can be neglected for modeling [18]. Reorientation times, τ_R, are known to depend on solvent polarity and molecular volumes [9,16,17]. In our measurements $\tau_R = 270 \pm 50$ ps for PD 2630 in ethanol, 130 ± 25 ps for SD 2243 in dichloromethane due to the lower viscosity of dichloromethane, and 550 ± 100 ps for TD 2765 (larger molecular volume) in ethanol. Note that $\tau_F > \tau_R$ for polymethine and squaraine but not for tetraone: τ_F (TD 2765) is nearly twice as short as τ_R in ethanol, consistent with a small fluorescence quantum yield (measured to be ~5 %, considerably smaller quantum yield than that of PD 2630 and SD 2243). The maximum anisotropy values for all dyes $r(0) \approx 0.37$–0.38 are in agreement with one-photon anisotropy measurements showing the nearly parallel orientation of the ESA transition moments to μ_{01}.

Open aperture picosecond Z-scan measurements are performed at 532 and 1064 nm with spot sizes calibrated using CS_2 as described previously in this section. At each wavelength the optical geometry was modified to maintain the "thin sample approximation" with 1 mm cells [11]. Inside the absorption band, at 532 nm, Z-scan's are modeled by reverse saturable absorption

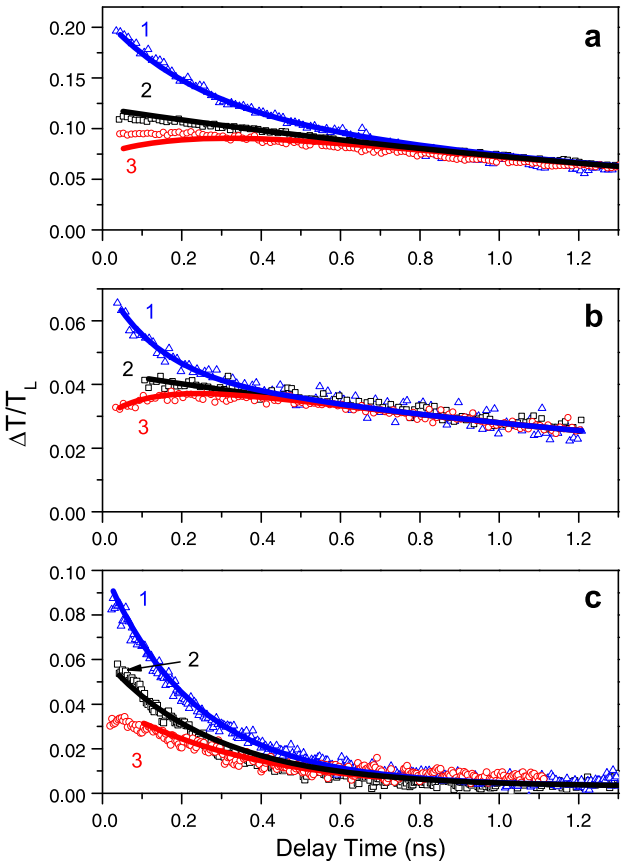

Fig. 5. Polarization H resolved picosecond pump–probe data for (a) PD 2630 in ethanol, (b) SD 2243 in dichloromethane, and (c) TD 2765 in ethanol. The orientations of the probe beam relative to the pump are: (1) perpendicular, (2) "magic angle" 54.7^0 and (3) parallel. Data are modeled using Eq. (2) in Section 2.2.

(RSA [3]), Fig. 6(a) and (b), to extract the ESA cross-section. The data are modeled by both four-level and three-level systems (singlet levels only) for several fluences. The three-level system sufficiently describes the nonlinear absorption for picosecond inputs at low fluences (typically less than 0.05 J/cm^2). Propagation and rate equations for the RSA model at 532 nm are described by Eq. (3):

$$\begin{aligned}
\frac{dI}{dz} &= -\sigma_{01}N_0 I - \sigma_{12}N_1 I \\
\frac{dN_0}{dt} &= -\frac{\sigma_{01}N_0 I}{\hbar\omega} + \frac{N_1}{\tau_F} \\
\frac{dN_1}{dt} &= \frac{\sigma_{01}N_0 I}{\hbar\omega} - \frac{N_1}{\tau_F} - \frac{\sigma_{12}N_1 I}{\hbar\omega} + \frac{N_2}{\tau_{21}} \\
\frac{dN_2}{dt} &= -\frac{\sigma_{12}N_1 I}{\hbar\omega} - \frac{N_2}{\tau_{21}}
\end{aligned} \tag{3}$$

where $N = N_0 + N_1 + N_2$, τ_F is determined from the pump–probe measurements (Fig. 5), and τ_{21} is the decay lifetime of the S_2 level. Data for 532 nm Z-scan's and their fitting with this model are shown in Fig. 6(a) and discussed in Section 3.3.

Outside the main absorption band at 1064 nm, Z-scan's are modeled with a simplified three-level system including ESA accessed by 2PA (with 2PA coefficient β) as shown in Fig. 6(c) and described by Eq. (4):

$$\begin{aligned}
\frac{dI}{dz} &= -\beta I^2 - \sigma_{12}NI \\
\frac{dN}{dt} &= \frac{\beta I^2}{2\hbar\omega} - \frac{N}{\tau_F}
\end{aligned} \tag{4}$$

For practical purposes, there are applications where the total nonlinear absorption, including 2PA with ESA, is of interest. The region from 950 to 1050 nm has significantly less 2PA for PD 2630 and SD 2243 as compared to TD 2765 as observed in Fig. 3, and it is therefore, interesting to study the nonlinear absorption involving multiple mechanisms, i.e. pure 2PA and 2PA followed by ESA. Each molecule is measured with at least four increasing irradiance levels by Z-scan resulting in a nonlinear transmittance change from ~2% to ~30%. For low input irradiance very good agreement is observed in the pure 2PA measured by two-photon fluorescence with femtosecond pulsewidths and Z-scan measurements performed with picosecond pulsewidths. For example, at 1064 nm, pure 2PA cross-sections, extracted from Eq. (4) using picosecond pulsewidths are 15, 6, and 126 GM for PD 2630, SD 2243, and TD 2765 and are in good agreement with the femtosecond 2PF measurements of 18, 6, and 109 GM, respectively. ESA cross-sections at this wavelength, accessed by 2PA, are found from fits to the picosecond measurements to be 2, 4, and 0.5×10^{-17} cm^2 for PD 2630, SD 2243, and TD 2765, respectively.

3. Discussion of results and quantum-chemical approach

3.1. 2PA spectra

Experimental one- and degenerate two-photon absorption spectra for PD 2630, SD 2243 and TD 2765 are presented in Fig. 3 with a semi-logarithmic scale for 2PA cross-section. For comparison with linear absorption, 2PA spectra are shown on the same graph by multiplying the wavelength scale by 2, with separate axes for 1PA (top) and 2PA (bottom). Both the polymethine and the squaraine dyes show two separated bands and the edge of a third 2PA band. The "first" band, as labeled in our previous papers [4,5], is now understood to be comprised of two overlapping bands: the lower energy band is due to vibrational coupling within the main absorption transition (2PA forbidden); the higher energy band corresponds to the lowest 2PA allowed transition. The largest 2PA cross-section measured for SD 2243, $\delta_{2PA} \approx 8500$ GM, is about 6.5 times larger than that for PD 2630. This is due to the larger ISRE resulting from the steeper linear absorption edge of the squaraine, allowing tuning closer to resonance, and from the increased density of final states introduced by the squaraine acceptor group [5]. The cross-section values at the second 2PA peak for both dyes are similar: $\delta_{2PA} \approx 1200$ GM for SD 2243 and $\delta_{2PA} \approx 1000$ GM for PD 2630. Both compounds show a sharp decrease in 2PA values at ≈500 nm (2PA excitation ≈1000 nm). The striking differences in the 2PA spectrum of the tetraone dye as compared with both the polymethine and squaraine are the evidence of three 2PA bands, the edge of a fourth 2PA band, and a nearly monotonic increase in 2PA cross-section (note the semi-logarithmic scale for 2PA). These bands strongly overlap the spectral range in 2PA from 1150 to 700 nm and eliminate the decrease in 2PA observed for PD 2630 and SD 2243. A similarly large 2PA at the edge of the fourth band $\delta_{2PA} \approx 8200$ GM is observed for the tetraone dye as compared to the squaraine. Our measurements for TD 2765 reveal the third band with a peak position at ≈410 nm (≈820 nm 2PA) with $\delta_{2PA} \approx 2700$ GM. A second new band connected with the introduction of the stronger acceptor bridge is observed at ≈480 nm (≈960 nm 2PA) with $\delta_{2PA} \approx 900$ GM. This band is not found in PD 2630 and SD 2243.

The nature of the first 2PA band (δ_{2PA} = 100–150 GM) in all three molecules is under further investigation. At this time, we believe that the band is comprised of two features. Experimentally this has been observed in several polymethines and squaraines in solvents of different polarity. The position of the first low-energy band always corresponds to the position of the

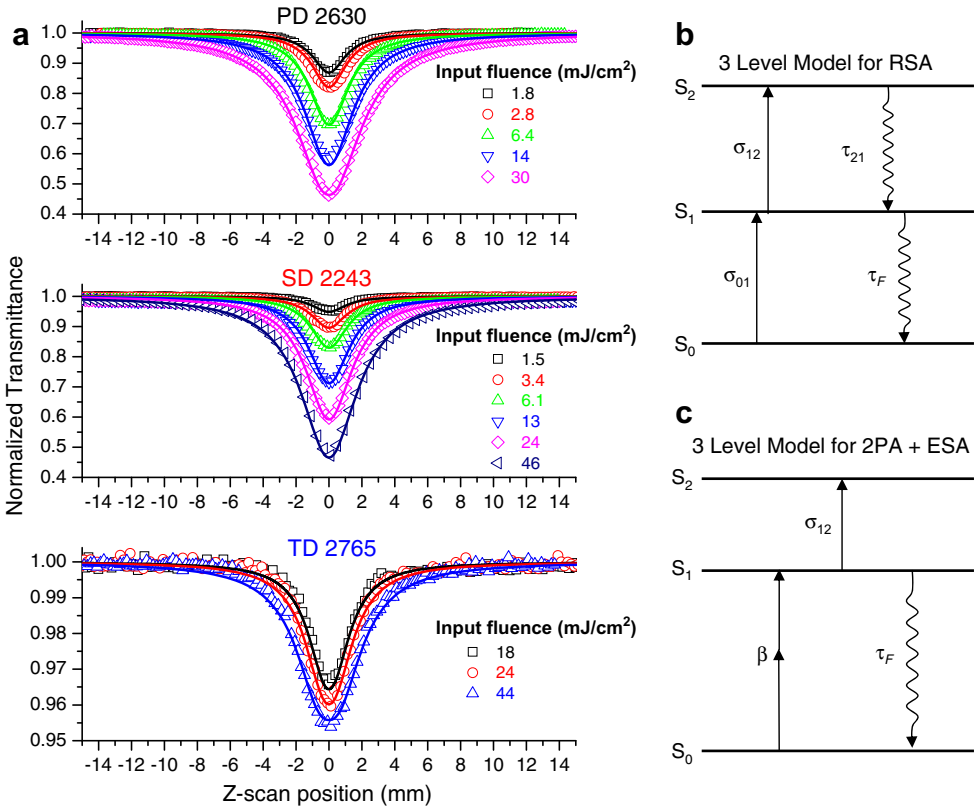

Fig. 6. (a) Typical picosecond *Z*-scan results at 532 nm for PD 2630, SD 2243, and TD 2765. Fitting curves are modeled by Eq. (3) in Section 2.2 and parameters and results are discussed in Section 3.3. (b) Schematic of three-level energy diagram for reverse saturable absorption. (c) Schematic of simplified three-level system for excited-state absorption accessed by two-photon absorption.

vibronic shoulder on the high energy side of the linear absorption band $S_0 \rightarrow S_1$. This weakly allowed 2PA within the main band is typically observed and explained by the effect of vibronic coupling partly breaking the molecular symmetry and thus the dipole selection rules [5,19]. However, we consistently observe an additional structure, blue shifted from this shoulder. Our quantum-chemical calculations for all three molecules predict the existence in this region of a one-photon forbidden electronic transition $S_0 \rightarrow S_2$. This has negligibly small oscillator strength and is overlapped with the $S_0 \rightarrow S_1$ vibrations. Therefore, we cannot resolve this in the excitation anisotropy spectra. We suppose that this high energy band could indicate the position of the lowest two-photon allowed electronic transition, see Section 3.2 for more details.

3.2. Quantum-chemical approach

Quantum-chemical analysis is performed with the goal of understanding the formation of 2PA and ESA bands and revealing the origin of the larger δ_{2PA} in squaraine and tetraone molecules as compared to polymethines. The methodology for the calculations of the positions of the electronic levels and the shapes of their molecular orbitals is described in Refs. [5,6].

Schemes of some higher occupied and lower unoccupied molecular orbitals (HOMO and LUMO), their shapes and corresponding transitions between them are presented in Figs. 7 and 8. In our considerations we limited the number of levels by the number of electronic transitions participating in one- and two-photon absorption between $S_0 \rightarrow S_1$ and twice that energy or "double resonance" position as described in more detail in Refs. [5,6].

3.2.1. Polymethine

Quantum-chemical analysis performed for PD 2630 shown in Figs. 7(a) and 8(a) allow distinction between three types of molecular orbitals: two donor orbitals HOMO and HOMO-1, originating from the donor nitrogen atoms; local occupied and unoccupied orbitals, placed primarily on the benzene rings of the terminal groups (HOMO-2, HOMO-3, HOMO-5, HOMO-6, LUMO+3, LUMO+4); and delocalized orbitals spreading out over the chain (LUMO, LUMO+1) or the entire molecule (HOMO-4). Note that symmetrical and asymmetrical pairs of donor and local orbitals are formed from the doubly degenerate orbitals as a result of their splitting, leading to charge redistribution, see Fig. 8. Therefore, corresponding transitions to these orbitals are characterized by very different oscillator strengths. For example, HOMO → LUMO ($1A_1 \rightarrow 1B_1$, C_{2V} molecular symmetry) corresponds to the intense long wavelength band in the one-photon absorption spectrum. The next transition involving mostly the pure asymmetrical donor HOMO-1 and asymmetrical delocalized LUMO and being of the $1A_1 \rightarrow 2A_1$ symmetry, corresponds to the lowest two-photon allowed transition and is characterized by a very small oscillator strength ≈0.02. Our calculations show that this transition is placed around 575 nm presumably corresponding to the lowest 2PA allowed transition. The next two-photon allowed transition $1A_1 \rightarrow 3A_1$ for PD 2630 corresponds to the electron transfer between the asymmetrical local HOMO-3 and asymmetrical delocalized LUMO in agreement with the experimental spectral position of the second 2PA band seen in Fig. 3 at ≈440 nm (≈880 nm 2PA). These data are in accord with our previous finding suggesting that the existence of the local molecular orbitals is of great importance for 2PA [5]. The next, third 2PA band, with a calculated peak position of ≈350 nm (≈700 nm 2PA), cannot be fully

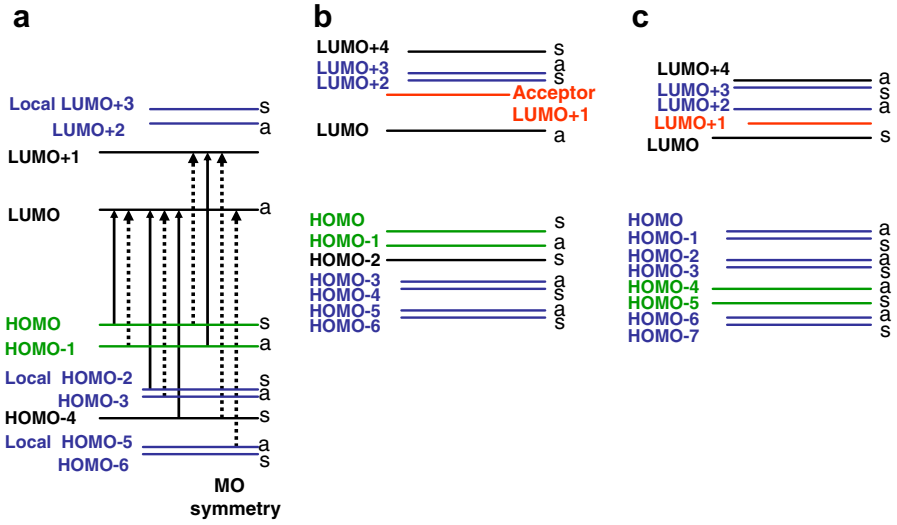

Fig. 7. Schematic of electronic levels for (a) PD 2630, (b) SD 2243 and (c) TD 2675. Green levels are MOs formed by donor nitrogen atoms, red – acceptor orbitals, blue – local orbitals formed by terminal groups, and black – delocalized orbitals. Vertical lines for PD 2630 indicate one-photon allowed (solid lines) and forbidden (dashed lines) transitions. (For interpretation of the references to color in this figure legend, the reader is referred to the web version of this article.)

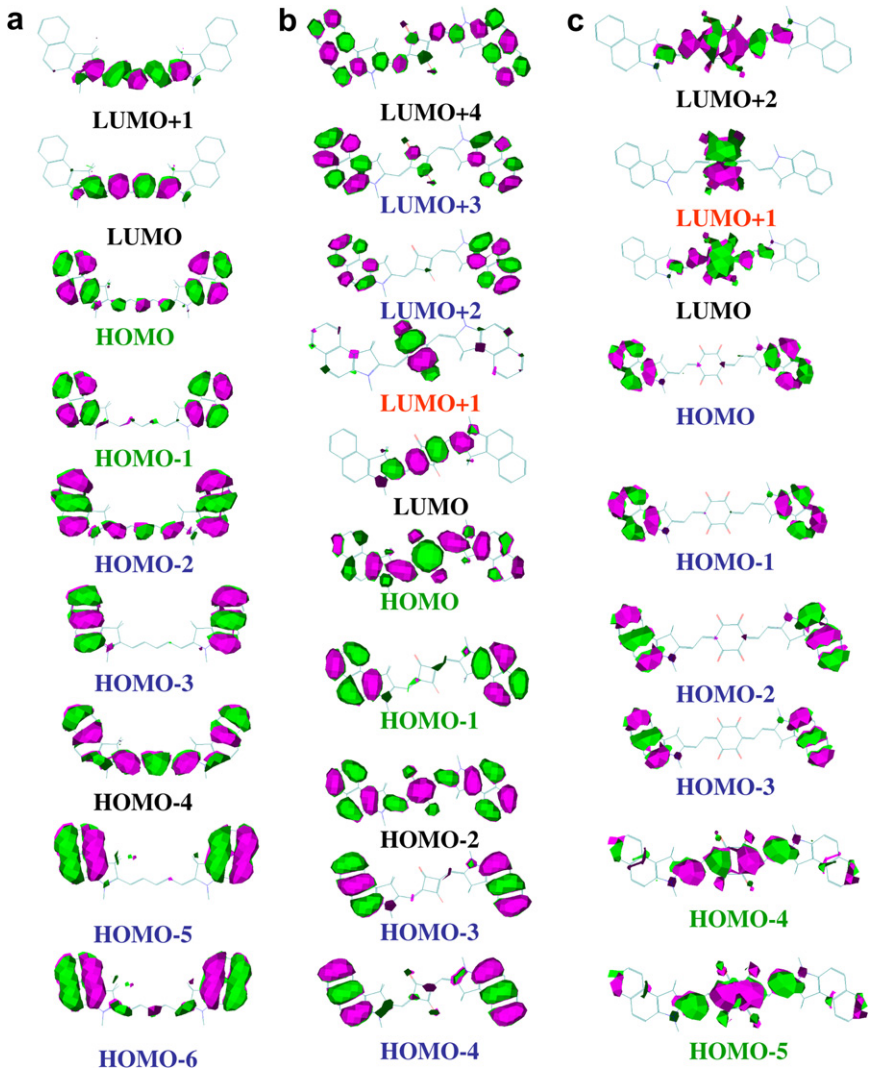

Fig. 8. Electron density distribution in the molecular orbitals for (a) PD 2350, (b) SD 2243 and (c) TD 2675.

experimentally resolved due to the linear absorption tail and corresponds to the mixed transition HOMO → LUMO+1 and HOMO-4 → LUMO+1. The beginning of this band is measured experimentally.

3.2.2. Squaraine

The electronic structure of squaraines has many similar features with polymethines such as the same polymethinic chain and the same degeneracy of the donor and local molecular orbitals. However, insertion of the acceptor C_4O_2 fragment in the center of the polymethine chain makes the SD-molecule formally neutral, or more correctly, bi-ionic with separated positive and negative charges. As a result, as shown in Fig. 7(b), the molecular orbitals are shifted to larger energies, and the distances between LUMOs become smaller, thereby increasing the density of unoccupied molecular orbitals as compare to the corresponding PD 2630. Therefore, the energies of the 2PA transitions involving LUMOs can be red shifted and experimentally attainable through the increased influence of the "double resonance" (as was shown for SD 2755 in Ref. [5]). The second distinguishing feature is the appearance of acceptor molecular orbital LUMO+1, for SD 2243 (see Fig. 8(b) for the charge distribution). The introduction of the acceptor fragment to the chain also leads to a reassembling of MOs: delocalized occupied orbital becomes HOMO-2 instead of HOMO-4 (as for PD 2630). In the case of SD 2243, four HOMO's and three LUMO's have to be considered to elucidate the nature of the allowed and forbidden transitions in the spectral region between the first transition and twice that energy, which can be measured by 2PA. The nature of the allowed $S_0 \rightarrow S_1$ transition for SD 2243 remains the same as for the polymethines and is connected with the electron transfer between symmetrical donor HOMO and asymmetrical delocalized LUMO. Similar to PD 2630, the asymmetrical donor HOMO-1 is involved in the lowest 2PA transition $1A_g \rightarrow 2A_g$ (C_{2i} molecular symmetry): HOMO-1 → LUMO. The next two-photon allowed transition $1A_g \rightarrow 3A_g$ for SD 2243 represents a mixed transition from the local HOMO-3 to LUMO+2 and HOMO-4 to LUMO+3. This band is observed experimentally at ≈440 nm (≈880 nm 2PA), see Fig. 3. The third 2PA band cannot be fully experimentally resolved, similar to PD 2630, and corresponds to the mixed transition from HOMO and HOMO-2 to LUMO+4. The increased density of LUMOs in squaraine decreases the detuning energy and increases the probability of 2PA to a final state, enhancing δ_{2PA} further.

3.2.3. Tetraone

The electronic structure of tetraone has similarities with both polymethines and squaraines: degeneracy of the donor and local molecular orbitals, an appearance of an unoccupied acceptor level, and a blue shift in energy of the MOs due to neutrality. The main distinguishing feature is a polyenic-like structure of the conjugated chain resulting in reordering of the levels. Figs. 7(c) and 8(c) present the order and the shapes of the MOs involving one- and two-photon transitions in the spectral range of interest. As compared to SD 2243, HOMOs of TD 2675 are changed in order: the first four orbitals are local with the charge distribution primarily on the benzene rings of the terminal groups, and the donor MOs become HOMO-4 and HOMO-5. Therefore, HOMO-4 → LUMO and HOMO-5 → LUMO transitions in tetraone are responsible for the first 1PA and 2PA bands. The LUMOs are also modified compared to SD 2243. They are characterized by a further increased density of unoccupied levels resulting in experimentally observed broadening of 2PA bands overlapping the spectral range in 2PA from 1150 to 700 nm as is observed in Fig. 3. Our calculations show that in contrast to polymethine and squaraine dyes, the second new two-photon allowed transition $1A_g \rightarrow 2A_g$ (C_{2i} molecular symmetry) corresponds to the charge transfer transition from the local HOMO-4 to the acceptor orbital LUMO+1. This band is found at ≈480 nm (≈960 nm 2PA), see Fig. 3. The nature of the third 2PA band is similar to the second 2PA band in PD 2630, and corresponds to the transition from the asymmetrical local HOMO to the asymmetrical delocalized LUMO+2. The experimentally observed edge of the fourth 2PA band corresponds to a mix of two transitions: HOMO-4 → LUMO+2 and HOMO-5 → LUMO with a calculated peak location at ≈450 nm (≈900 nm 2PA).

3.3. ESA–2PA link

Quantum-chemical calculations and molecular orbital analysis allow estimation of the positions of the ESA bands, their orientation relative to the main band, $S_0 \rightarrow S_1$, as well as the MOs which are responsible for the ESA magnitude. These ESA transitions can be roughly calculated as the energy difference between the positions of the 2PA peaks and the main linear absorption peak assuming that there are no essential changes in the excited-state molecular geometry upon excitation. For cyanine-like molecules the intramolecular relaxation upon excitation is small as evidenced by the small Stokes shifts and nearly mirror symmetry in the absorption and fluorescence spectra. Experimentally measured ESA bands for PD 2630, SD 2243 and TD 2765 are shown in Fig. 4.

According to our calculations, for PD 2630 there are six allowed ESA bands ($1B_1 \rightarrow nA_1$ symmetry) of different intensity in the spectral range 400–3500 nm. Weak ESA bands, corresponding mainly to overlapping between HOMO-1, HOMO-3 and HOMO-5 and HOMO are placed in the range 3500, 1300 and 650 nm. All intense ESA bands correspond to LUMO → LUMO+1 transitions involving MOs with π-delocalization oriented only along the polymethine chain as in the unsubstituted molecule. Their calculated spectral positions are: 720, 525 and 450 nm. Two ESA bands, placed in the range of transparency of PD 2630 with the peak positions around 530 and 420 nm, are found experimentally in very good agreement with theoretical predictions, see Fig. 4(1′). The ESA band at 720 nm is situated in the region near the fluorescence maximum and cannot be observed in femtosecond pump–probe experiments due to the strong stimulated emission cross-section.

Similar analysis is applied to SD 2243. Weakly allowed ESA bands $1B_u \rightarrow nA_g$ are predicted at 3500 and 1400 nm, and intense ESA bands corresponding to transitions between delocalized orbitals LUMO → LUMO+4 at wavelengths of 850, 550 and 460 nm, analogous to PD 2630. Experimentally measured ESA bands for SD 2243 in dichloromethane, presented in Fig. 4(2′), are also in agreement with theoretical findings. We note that weak ESA bands around 1380 and 870 nm for SD 2243 in ethanol were experimentally observed in our earlier work in good agreement with theoretical predictions [15].

For TD 2765 the first weakly allowed ESA band $1B_u \rightarrow nA_g$ is predicted in the infrared spectral vicinity of 4500 nm, and the second band is expected approximately in the same region as for polymethine and squaraine at ~1400 nm. More intense ESA bands corresponding to transitions between delocalized orbitals LUMO → LUMO+2 are predicted at wavelengths of 830, 520 and 420 nm. As seen in Fig. 4(3′), the ESA band in tetraone does not have two pronounced peaks in the visible as predicted by our calculations, but they are contained in one broad peak between 400 and 540 nm.

Concluding the experimental and theoretical results related to the ESA spectra, we find that all intense bands in the visible region for polymethine and tetraone dyes have a similar nature. They are connected with the transition between molecular orbitals delocalized only within the chain as in the unsubstituted molecules and are insensitive to the terminal groups. For squaraine dye, these intense ESA transitions are transitions between delocalized orbitals LUMO → LUMO+4. The only difference is that the LUMO+4 orbital

is delocalized within the entire molecule. This theoretical finding may be useful for the design of molecules with strong ESA for nonlinear transmittance applications.

Picosecond *Z*-scan measurements at 532 nm, as described in Section 2.2, allow for the determination of excited to ground-state cross-section ratios and differences, σ_{1i}/σ_{01}, and $\sigma_{1i} - \sigma_{01}$, parameters important for nonlinear transmittance. To our knowledge, the largest $\sigma_{1i}/\sigma_{01} \approx 200$ (while keeping $\sigma_{01} \approx 1.5 \times 10^{-18}\,\mathrm{cm}^2$) for a particular polymethine dye was measured previously by our group [20]. Our calculations for PD 2630, SD 2243 and TD 2765 give the following values for $\sigma_{1i}(532)$: 2.6×10^{-16}, 1.1×10^{-16} and $1 \times 10^{-16}\,\mathrm{cm}^2$, respectively. At 532 nm this data corresponds to σ_{1i}/σ_{01} ratios of 18, 23, and 1.1 for the polymethine, squaraine, and tetraone dyes, respectively. The peak σ_{1i}/σ_{01} for PD 2630, SD 2243, and TD 2765 correspond to 23 at 520 nm, 32 at 510 nm, and 8 at 480 nm. *Z*-scan measurements at 1064 nm show that the excited-state cross-sections in the near infrared region are smaller than in the visible, especially for TD 2765: 2×10^{-17} (for PD 2630), 4×10^{-17} (for SD 2243), and $0.5 \times 10^{-17}\,\mathrm{cm}^2$ (for TD 2765). However, the two-photon cross-section for TD 2765 at 1064 nm is much larger than for polymethine and squaraine: $\delta_{2PA} \approx 15$ GM for PD 2630, 6 GM for SD 2243 and 126 GM for TD 2765, and are in good agreement with the femtosecond 2PF measurements of 18, 6, and 109 GM.

4. Conclusions

We have described a detailed experimental investigation and quantum-chemical analysis of the 2PA and ESA spectra of a symmetrical cationic polymethine, a neutral squaraine, and a tetraone dye having similar structures. From these measurements, we find that, in the spectral region between the first absorption band and twice that energy, there are two 2PA bands and the tail of a third 2PA band for PD 2630 and SD 2243, and three 2PA bands and the beginning of an intense forth 2PA band for TD 2765. For the ESA spectra, bands appear in the visible range between 400 and 600 nm. Experimental and quantum-chemical analysis allowed us to make the following conclusions:

1. For all these molecules we observed a weakly allowed 2PA band within the vibronic shoulder of the first absorption band $S_0 \rightarrow S_1$ with $\delta_{2PA} \approx 100$–150 GM. We suppose that this "first" band is comprised of two overlapping bands: the lower energy band is due to vibrational coupling within the main absorption transition (2PA forbidden); the higher energy band corresponds to the lowest 2PA allowed transition.
2. Introduction of the acceptor group to the conjugated chain significantly increases the density of final states and thus the number of possible electronic transitions between the first band, $S_0 \rightarrow S_1$, and twice that energy. Additionally, for squaraine molecules, we observe a large intermediate state resonance enhancement due to a narrower linear absorption spectra. These factors are responsible for the large 2PA (more than 8200 GM) which is achieved for both SD 2243 and TD 2765. The distinguishing feature of TD is the experimentally observed broadening of 2PA bands overlapping the broad spectral range from 1150 to 700 nm.
3. Quantum-chemical calculations and molecular orbital analysis allow estimation of the positions of the ESA bands, their strength and dipole orientation relative to that of the main band $S_0 \rightarrow S_1$. The strongest ESA bands situated in the visible region are measured experimentally and are found to be connected with the transition between delocalized molecular orbitals.

These studies have advanced our understanding of the structure–property relations for nonlinear absorption in conjugated cyanine-like molecules to a level where our quantum-chemical calculations are in excellent agreement with experiments over a broad spectral range from 1400 to 700 nm for 2PA and 1400 to 400 nm for ESA. As 2PA is determined in perturbation theory from a sum over all sequential linear absorption processes that include ESA, we are making significant progress towards a predictive capability for the nonlinear absorption properties of this class of organic molecules.

Acknowledgements

We gratefully acknowledge the support of the National Science Foundation ECS 0524533, the US Army Research Laboratory W911NF0420012, and ARO MURI W911NF0610283.

References

[1] R.S. Lepkowicz, O.V. Przhonska, J.M. Hales, D.J. Hagan, E.W. Van Stryland, M.V. Bondar, Yu.L. Slominsky, A.D. Kachkovski, Chem. Phys. 286 (2003) 277.
[2] J. Fu, O.V. Przhonska, L.A. Padilha, D.J. Hagan, E.W. Van Stryland, K.D. Belfield, M.V. Bondar, Yu.L. Slominsky, A.D. Kachkovski, Chem. Phys. 321 (2006) 257.
[3] R.S. Lepkowicz, O.V. Przhonska, J.M. Hales, D.J. Hagan, E.W. Van Stryland, M.V. Bondar, Yu.L. Slominsky, A.D. Kachkovski, JOSA B 22 (2005) 2664.
[4] J. Fu, L.A. Padilha, D.J. Hagan, E.W. Van Stryland, O.V. Przhonska, M.V. Bondar, Yu.L. Slominsky, A.D. Kachkovski, JOSA B 24 (2007) 56.
[5] J. Fu, L.A. Padilha, D.J. Hagan, E.W. Van Stryland, O.V. Przhonska, M.V. Bondar, Yu.L. Slominsky, A.D. Kachkovski, JOSA B 24 (2007) 67.
[6] S.-J. Chung, S. Zheng, T. Odani, L. Beverina, J. Fu, L.A. Padilha, A. Biesso, J.M. Hales, X. Zhan, K. Schmidt, A. Ye, E. Zojer, S. Barlow, D.J. Hagan, E.W. Van Stryland, Y. Yi, Z. Shuai, G.A. Pagani, J.-L. Bredas, J.W. Perry, S.R. Marder, J. Am. Chem. Soc. 128 (2006) 14444.
[7] E. Zojer, D. Beljonne, P. Pacher, J.-L. Bredas, Chem. Eur. J. 10 (2004) 2668.
[8] T. Kogej, D. Beljonne, F. Meyers, J.W. Perry, S.R. Marder, J.-L. Bredas, Chem. Phys. Lett. 298 (1998) 1.
[9] J.R. Lakowicz, Principles of Fluorescence Spectroscopy, Kluwer Academic/Plenum Publishers, New York, 1999.
[10] J.-C. Diels, E.W. Van Stryland, D. Gold, in: C.V. Shank, E.P. Ippen, S.L. Shapiro (Eds.), Picosecond Phenomena, vol. 117, Springer-Verlag, 1978.
[11] M. Sheik-Bahae, A.A. Said, E.W. Van Stryland, Opt. Lett. 14 (1989) 955.
[12] C. Xu, W.W. Webb, JOSA B 13 (1996) 481.
[13] M. Sheik-Bahae, A.A. Said, T.-H. Wei, D.R. Hagan, E.W. Van Stryland, IEEE J. Quant. Electron. 26 (1990) 760.
[14] M. Fisher, J. Georges, Chem. Phys. Lett. 260 (1996) 115.
[15] R.A. Negres, O.V. Przhonska, D.J. Hagan, E.W. Van Stryland, M.V. Bondar, Yu.L. Slominsky, A.D. Kachkovski, IEEE J. Quant. Electron. 7 (2001) 849.
[16] R.S. Lepkowicz, O.V. Przhonska, J.M. Hales, J. Fu, D.J. Hagan, E.W. Van Stryland, M.V. Bondar, Yu.L. Slominsky, A.D. Kachkovski, Chem. Phys. 305 (2004) 259.
[17] O.V. Przhonska, D.J. Hagan, E. Novikov, R.S. Lepkowicz, E.W. Van Stryland, M.V. Bondar, Yu.L. Slominsky, A.D. Kachkovski, Chem. Phys. 273 (2001) 235.
[18] R.W. Redmond, I.E. Kochevar, M. Krieg, G. Smith, W. Grant McGimpsey, J. Phys. Chem. A 101 (1997) 2773.
[19] D. Scherer, R. Dorfler, A. Feldner, T. Vogtmann, M. Schwoerer, U. Lawrentz, W. Grahn, C. Lambert, Chem. Phys. 279 (2002) 179.
[20] J. Lim, O.V. Przhonska, S. Khodja, S. Yang, T.S. Ross, D.J. Hagan, E.W. Van Stryland, M.V. Bondar, Yu.L. Slominsky, A.D. Kachkovski, Chem. Phys. 245 (1999) 79.